Photochemical vs. photocatalytic azo-dye removal in a pilot Free-Surface Reactor: is the catalyst effective?

Elnaz Bahadori [a], Matthias Rapf [b], Alessandro Di Michele [c], Ilenia Rossetti [a*]

[a] Chemical Plants and Industrial Chemistry Group, Dip. Chimica, Università degli Studi di Milano, CNR-ISTM and INSTM Unit Milano-Università, via C. Golgi 19, 20133 Milano, Italy

[b] Research Group Resources Management and Industrial Wastes, Institute for Sanitary Engineering, Water Quality and Solid Waste Management, University of Stuttgart Bandtaele 2, 70569 Stuttgart, Germany

[c] Dip. di Fisica - Università degli Studi di Perugia, Via Pascoli, 06123 Perugia

Abstract

Advanced oxidation processes (AOPs) are potential alternatives for treatment of effluents containing hardly biodegradable textile dyes. These processes imply the generation and subsequent reaction of hydroxyl radicals (OH•), which are some of the most powerful oxidizing species. Among AOPs, ozonation (often combined with H_2O_2, UV, or both), showed to be promising either for the complete mineralization of dyes or for their transformation into less complex and more easily biodegradable structures.

In this study, the photocatalytic degradation of Levafix Brilliant Red E-6BA reactive textile dye has been investigated in presence of H_2O_2 by means of a Free-Surface Reactor (FSR), with two

---

[*] Corresponding author: email ilenia.rossetti@unimi.it; fax +390250314300

types of Hg lamps (Medium Pressure, MP, and Low Pressure, LP) irradiating the liquid from the top of the reactor without direct contact with the liquid. The dye degradation efficiency of the process has been evaluated by comparing the reaction rate constants (RRC) from experimental data and the total power consumption for wastewater treatment (R_{WW}). In order to increase the photodegradation efficiency, several TiO_2 based photocatalysts (TiO_2 commercial or prepared by Flame Spray Pyrolysis (FSP), bare or loaded with 0.1 mol% Pd or Au) have been added to the batch system.

The results suggest that the MP UV-FSR requires less energy for dye removal in case of high dye concentration, whereas, for lower dye concentration, LP UV-FSR shows better performance in terms of energy consumption. Bare P25 even in relatively low quantity (100 mg/dm^3) showed to be an active co-adjuvant for dye decoloration and aromatic structures degradation with half the energy consumption than a solution without photocatalyst.

1. Introduction

Textile industries consume enormous quantity of water and chemicals for finishing and dying processes. Most of the textile dyes have complicated aromatic structures with high resistance to the conventional wastewater treatment processes because of their stability to sunlight, oxidizing agents and microorganisms [1]. Therefore, from an environmental point of view, dyes removal from industrial effluents is one of the major concerns, which imposes a stringent legislation for the textile industry. Azo dyes and their degradation products include a huge number of contaminants with toxic, mutagenic or carcinogenic effect on living organisms.

So far, many methods have been used to treat the wastewater, such as coagulation and flocculation [2–4], the chemical oxidation including Fenton's reagent [5–9], ClO_2, $NaClO$ or O_3 [10], air flotation processes adsorption by resins or activated carbon, activated sludge, anaerobic-aerobic two stage biochemical process [11], electrolytic [12,13] and high impulse current. Most of the mentioned techniques are only able to remove the color, *i.e.* breaking the N-containing bond which guarantees electron mobility across the molecule, without achieving the total degradation (mineralization) of toxic intermediates. The limitations of conventional biological or chemical oxidation techniques can be overcome by the development of the so-called advanced oxidation processes (AOPs), which can be standalone or combined with other techniques [14]. AOPs mainly involve the generation of very strong oxidizing species, but relatively non selective. Primarily, it means hydroxyl ($\bullet$OH) radicals, formed through radical chain photo-induced decomposition of hydrogen peroxide in pure water (equations 1-7), which in turn increases the degradation of organic contaminants into harmless inorganic substances such as CO_2 and H_2O under mild conditions (full mineralization) [15]. One of the oldest and commercially available AOP methods

is the UV/H₂O₂ method. H₂O₂ is easy to handle in aqueous solutions and is a powerful oxidant and a source of (•OH) radicals.

1. $Initiation: H_2O_2 + h\upsilon \rightarrow 2 \bullet OH$

2. $Propagation: H_2O_2 + \bullet OH \rightarrow H_2O + HO_2\bullet$

3. $HO_2 \bullet + H_2O_2 \rightarrow H_2O + \bullet O_2 \bullet + \bullet OH$

4. $Net\ Reaction: 2H_2O_2 \rightarrow 2H_2O + \bullet O_2 \bullet$

5. $Termination: HO \bullet + \bullet OH \rightarrow H_2O_2$

6. $HO \bullet + HO_2 \bullet \rightarrow H_2O + \bullet O_2 \bullet$

7. $HO_2 \bullet + \bullet O_2H \rightarrow H_2O_2 + \bullet O_2 \bullet$

Although AOPs include very often photocatalytic methods activated by UV-light, recent studies focus on solar light energy as a more challenging issue [16]. In this regard, heterogeneous photocatalysis, such as UV-TiO₂-based solar catalytic oxidation system, reveals some attractive characteristics [17]. Titanium dioxide (TiO₂) is an inexpensive, non-toxic and environmentally friendly semiconductor, with high structural stability and is insoluble in aqueous solution. Furthermore, the band gap of this material (3.2 eV) and band energy positions provide a high photoactivity towards the degradation of many highly concerning molecules, with a further possibility to exploit solar light for several applications, such as the treatment of organics [18–20] and dye [19–22] pollutants from water. Since only a small fraction (about 3–5%) of the solar spectrum constitutes the UV light, research efforts focused on the goal of shifting the optical response of TiO₂ toward visible light and enhancing its photocatalytic activity by incorporating transition metal oxides (such as Fe, Zn, Cu, Ni and V) [26–28] or noble metals (such as Au, Pd, Ag and Pt) [25,29–32]. Some of these metals, *e.g.* Au and Pd, can improve light harvesting of the TiO₂ thanks to plasmonic resonance in the visible region. In other cases, depending on the

workfunction, the metal nanoparticles distributed on the surface as co-catalyst may act as a sink for the photo-promoted electrons, allowing to improve the lifetime of the photo-generated charges. In the field of azo-dyes removal, a lot of investigations deal with either homogeneous or heterogeneous light-supported approaches, mainly focusing on the development of new photocatalysts or checking the effect of operating conditions. Pilot scale studies are only few [33–35] and, furthermore, a homogeneous comparison of the two approaches is missing and no attempts to conceptualise the possible scale up of the technologies is currently available. Elements of choice must be the conversion achievable as a function of time, of course, but also elements to ascertain the scalability of the processes and their economic impact.

Therefore, in this study, the efficiency of a H_2O_2/UV process for the removal of Levafix Brilliant Red E-6BA reactive dye effluent is investigated. A Free-Surface Reactor (FSR) was used for testing. A pilot scale photoreactor (10 L capacity) has been tested for the first time, comparing a photochemical *vs*. photocatalytic AOP approach as example of rival technologies, characterized by different cost of reactants, catalysts and power consumption. To check the effect of the operating conditions on the dye removal efficiency, two main parameters were calculated: the Reaction Rate Constant (RRC, 1/h) and the total energy consumption for wastewater treatment (R_{ww}, kWh/m^3), so comparing the feasibility of the technologies proposed with an applicative purpose. Different experimental parameters have been considered, such as the effect of H_2O_2 amount, dye concentration, the selection of different light sources, *e.g.* a medium pressure (MP) or low pressure (LP) Hg lamp with different power.

The photocatalytic efficiency for dye removal in the presence of commercial TiO_2 (Evonink P25) has been studied in comparison with TiO_2 obtained by flame spray pyrolysis (FSP), either bare or

added with gold (0.1 mol% Au-P25) or palladium (0.1 mol% Pd-P25, 0.1 mol% Pd-FSP), never applied for this reaction.

2. Experimental

2.1. Catalysts preparation

The commercial P25 sample supplied by Evonik (code P25) was used as a benchmark and its photocatalytic performance has been compared with TiO_2 samples prepared in dense nanoparticles form by Flame Spray Pyrolysis (FSP) [36–38]. The FSP samples were prepared by means of a home-developed device, composed of a burner, which is co-fed with the titania precursor solution and 5 L/min of oxygen. The flame is ignited and sustained by a ring of flamelets (0.5 L/min CH_4 + 1 L/min of O_2). A syringe pump at constant feeding rate of 2.5×10^{-3} L/min has been used for feeding the solution of the oxide precursor in organic solvent to the burner. Titanium Isopropoxide (Sigma Aldrich, pur. 97%) was dissolved into p-Xylene and Propionic acid (Sigma Aldrich, pur. 97%) with a 0.4 M concentration. The pressure drop at the burner nozzle was set to 1.5 bar [39–42].

The gold-promoted TiO_2 samples (0.1 mol% Au-P25) were prepared by a modified deposition-precipitation method using $AuCl_3$ 11.4 mg and 3 g of commercial TiO_2 (Evonik P25, 50 m^2/g) [43–46]. These compounds were dispersed in bi-distilled water (just enough to cover the solid particles).

Then the suspension was left under vigorous stirring for 1h at room temperature. Water was then removed under mild vacuum and the collected samples were dried overnight in oven (100 °C). Atomic Absorption Spectroscopy (AAS) analysis (Perkin Elmer 3100 instrument) was performed to assess the final composition which resulted the same as the nominal one.

An aqueous solution of $Pd(NO_3)_2$ was used as a precursor for the Pd nanoparticles with 0.1 mol % loading, added by impregnation on both P25 and FSP samples. Pd reduction was obtained in H_2 flow at 300 °C for 3h, according to preliminary Temperature Programmed Reduction (TPR). The metal loading has been optimised for a different application in the case of Au and kept fixed for comparison in the case of Pd.

2.2. Characterization techniques

Nitrogen adsorption/desorption isotherms were collected at -196°C on a Micromeritics ASAP2020 instrument on samples after pretreatment in vacuum at 300°C overnight.

X-ray diffraction (XRD) experiments were performed on a Rigaku D III-MAX horizontal-scan powder diffractometer with Cu-Kα radiation, equipped with a graphite monochromator on the diffracted beam.

Reflectance (DR) UV-Vis spectra of powder photocatalyst samples were measured on a Cary 5000 UV-Vis-NIR spectrophotometer (Varian instruments) in the range of 200–800 nm, in order to study the effect of metal doping on the light absorption nature and the band gap of materials.

TPR analysis was carried out on a bench scale apparatus by flowing 40 cm^3/min of a 10 vol% H_2/N_2 mixture, while heating the sample by 10 °C/min up to 700°C for 3h. The gas outflowing the quartz reactor was analysed by with a TCD detector after entrapping the possibly formed water.

The electrophoretic mobility of samples P25 and FSP was measured at 25°C as a function of pH, by means of electrophoretic light scattering technique on a Zetasizer Nano-ZS (Malvern Instruments, Worcestershire, UK). Water suspensions were sonicated for 2 min with an ultrasonic probe (400 W, 24 kHz, UP400S, Hielscher; Germany); the pH of the suspension was then adjusted by adding either 0.10 M HCl or 0.10 M NaOH.

2.3. Photoreactor design and test condition

The UV Free-Surface Reactor (UV-FSR) developed at the Institute for Sanitary Engineering, Water Quality and Solid Waste Management (ISWA) of the University of Stuttgart, has been used for all the experimental activity tests. The UV FSR (Figure 1), is basically an STR (stirred tank reactor) working in continuous or batch mode, with part of its surface irradiated by one or several UV lamps. Intensive stirring throughout the process provides almost ideally turbulent conditions in the aqueous reactor content. This results in a constantly renewed surface, allowing water or contaminants to meet statistically the photon source, independently from color and turbidity of the suspension or solution. The following Figure displays a schematic diagram of the reactor used for the experiments and some relevant technical specifications of the pilot scale 10 L FSR are listed in Table 1.
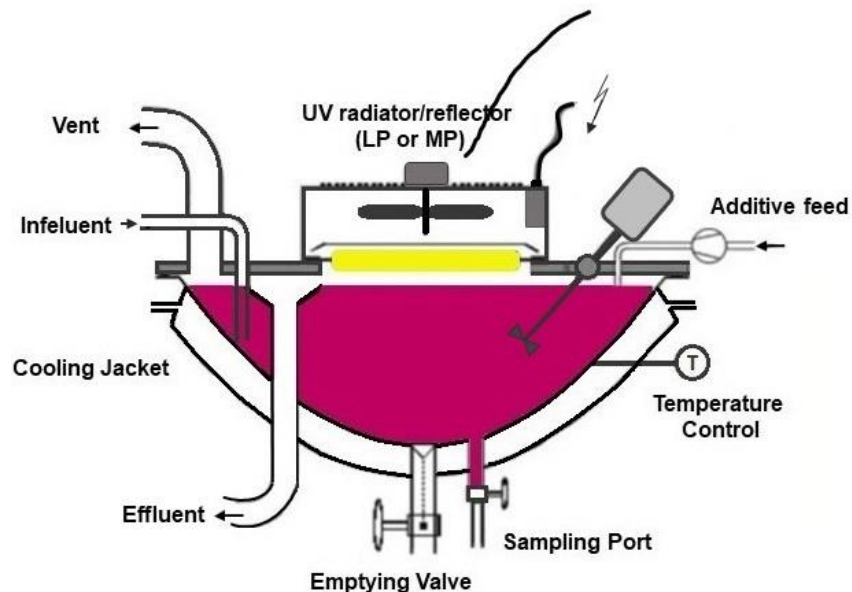

Figure 1: The 10 liters UV Free-Surface Reactor (UV-FSR) for batch or continuous operation [47]

Table 1: Technical specifications of the laboratory scale FSR with 2 different lamp types

Reactor type	double jacket UV Free-surface reactor, made of glass
Reaction volume	10 L
Distance between UV-radiator and wastewater surface	*ca.* 3 cm
Agitation	Mechanical stirrer with adjustable speed, set at 450 RPM for this experiment
Temperature	Water-cooled double jacket controls the temperature. The average temperature was *ca.* 20 °C for all tests
Hg lamps	LP Hg Lamp: • Six LP-UV lamps, each 10 cm length • Monochromatic • Maximum emission peak at 254 nm • Input power 210 W • UV-C efficiency is 35-40% of total electrical input power • Useful life time: 8000-12000 h MP Hg Lamp: • Single lamp with 10 cm length • Polychromatic • Emitting in a range of 200-280 nm • Input power 1700 W • UV-C efficiency is 15-18% of total electrical input power • Useful life time: 1500-4000 h
Lamp cooling system	Air ventilation

Levafix Brilliant Red E-6BA red was selected as a proper reactive dye for this experiment. This dye is an anionic, mono-functional reactive dye, very popular in the textile industry. It is hardly

biodegradable with high solubility in water, a high Chemical Oxygen Demand (COD) and a very low Biochemical Oxygen Demand (BOD5) (Table 2).

Table 2: Physical and chemical properties of Levafix Brilliant red E-6BA[*]

Chemical composition	$C_{32}H_{18}ClF_2LiN_6Na_2O_{11}S_3$
Solubility in water	70 g/dm^3
Chemical Oxygen Demand (COD)	965 mg/g
Biochemical Oxygen Demand (BOD$_5$[**])	< 30 mg/g [***]
Wavelength of maximum absorption	440-445 nm
Molecular weight	885.0843 g/mol
Bulk density	350-570 kg/m^3

*According to DyStar Colors Distribution GmbH, 2011, manufacturer database
** 5-day Biochemical Oxygen Demand
*** According to the index of water quality classification BOD > 5 mg/dm^3 O$_2$ is referred as contaminated water [48]

According to the COD, which gives the information on the oxygen demand for the total oxidation of the wastewater [49], the stoichiometric factors for the ratio COD:H$_2$O$_2$ has been calculated based on dye concentration, by assuming the efficient production of one OH• from each molecule of H$_2$O$_2$ [15]. Consequently, factors F = 1.0 (stoichiometric conditions), < 1.0 (sub-stoichiometric conditions) and Factor > 1.0 (over-stoichiometric conditions), mean that the oxygen demand by H$_2$O$_2$ is theoretically covered, not fully covered and covered in excess, respectively.

Tests were carried out in 10 L aqueous solution (derived from tap water) of Levafix Brilliant Red E-6BA (purity grade > 99.0%; initial concentration = 100 mg/dm^3; initial pH ~ 7.5) in the FSR. Two types of Hg lamps were used: One radiator/reflector unit contains six low pressure (LP) UV-radiators with the length of 10 cm and input power of 35 W for each lamp (total input power of 210 W), the other radiator/reflector unit contains one single medium pressure (MP) UV-radiator with the length of 10 cm and an input power of 1700 W (Table 1). Using the MP radiator (surface

temperature ~900°C), the solution was cooled down by means of water circulation in the outer compartment of the double jacket reactor, in order to not exceed a reactor temperature of 20 °C. A mechanical stirrer was located inside the reactor and adjusted to 450 rounds per minute to ensure suitable and uniform agitation of the liquid medium and constant renewal of the irradiated surface at the same time.

The first round of tests (Test 1-6) were performed without addition of catalyst, by varying different factors: *i)* dye concentration (10-150 mg/dm^3), *ii)* the H_2O_2 (50 wt%) amount as oxidation agent, based on different stoichiometry factors (F = 1 - 5.8) and *iii)* the MP Hg lamp and LP Hg lamp as irradiation sources. These results are reported based on the unpublished study, which have been produced by University of Stuttgart in previous experiments. The first three experiments were perfumed using the MP Hg lamp, in which in the two of the experiments 10 mg/dm^3 was selected as an initial dye concentration. Based on the calculated COD driving from dye concentration, the H_2O_2 was added with F = 1.0 (stoichiometric conditions), F=5.8 (over-stoichiometric conditions). The third test was carried out with 150 mg/dm^3 of dye concentration with F= 5.8 as a H_2O_2 addition stoichiometric factor.

The further three experiments were performed under the same experimental conditions varying only the irradiation source using LP Hg lamp.

In the second round of tests, 8 experiments were performed using only the MP Hg lamp to compare the effect of catalyst doping on dye degradation, and the results were compared with the blank test without catalysts (tests 7-14). The photocatalytic tests were performed using different catalysts (FSP, 0.1 mol% Pd-FSP,1 mol% Pd-P25 and 0.1 mol% Au-P25) all in the same amount (50 mg/dm^3). The initial dye concentration of 100 mg/dm^3 and the H_2O_2 (50 wt%) with fixed stoichiometric factor (F=1.8) were selected for all tests. The initial dye concentration C_0 (before

turning on the UV lamp) was measured at time t = 0. The best catalyst in terms of discoloration

and RRC then was selected to find the optimum dosage (in three different concentrations: 25, 50

and 100 mg/dm^3) in a same condition as before.

Two Perkin Elmer Lambda XLS+ and Lambda 35 spectrophotometers were used to measure the

Levafix Brilliant Red E-6BA concentration at its λ_{max} =542 nm in order to follow the degradation

kinetics. Samples were taken every 5 min for a total reaction time of 90 min, and photometry has

been performed in a 1 cm quartz cuvette. The maximum experimental error in the determination

of absorbance was 3%.

3. Results and discussion

3.1. Materials characterization

The XRD pattern of all samples show a mixture of the crystalline phases of anatase and rutile. All

the reflections were identified by comparison with the standard JCPDS spectrum of rutile (file 88-

1175) and anatase (file 84-1286) [50]. The FSP sample showed similar composition and particle

size with respect to P25 (Figure 2 and Table 3). The phase composition and the average particle

size of each sample have been estimated from the intensity ratio between the reflection of anatase

and rutile planes at (101) and (110) respectively (Table 3) [51]. The particle size of TiO_2 samples

has been calculated by using the Scherrer's equation [52] and reported in Table 3. The addition of

so small co-catalyst amount did not induce the segregation of separate Au or Pd-based phases. The

metal was found dispersed in small nanoparticles corresponding to the nominal amount. According

to the detailed characterization of the same Au and Pd loaded TiO_2 for a different photocatalytic

reaction, *i.e.* the photoreduction of CO_2 to solar fuels and of nitrates in waste water [46,53,54], the co-catalyst was found dispersed in form of fine nanoparticles. Au, in particular, was confirmed by high-resolution transmission electron microscopy (HRTEM) and scanning transmission electron microscopy (STEM) as dispersed in narrow particle size distribution (3.7-4.6 nm). X-ray photoelectron spectroscopy (XPS) also confirmed the nominal surface amount of Au in metallic form Au^0 (BE = 83 eV) without any detectable Au^{n+} species (BE = 85.5 eV) [46].
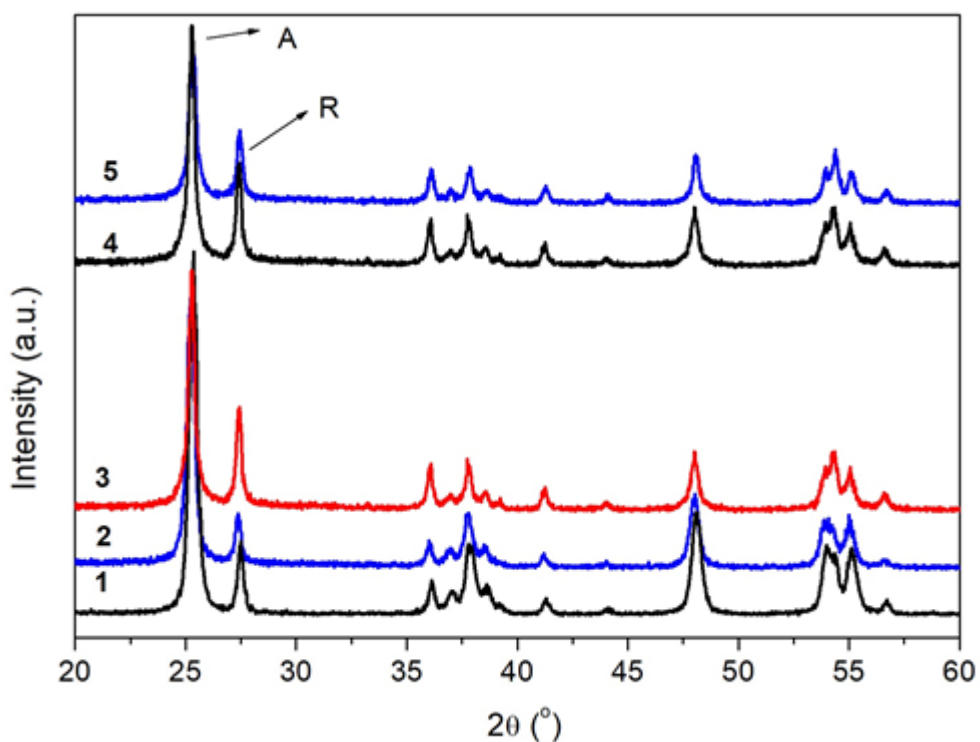
Figure 2: XRD patterns of (1) P25, (2) 0.1% Pd-P25, (3) 0.1% Au-P25, (4) FSP and (5) 0.1% Pd-FSP. A and R stand for the main reflections of anatase and rutile phases, respectively. Blue curves: Pd-loaded catalysts; red curve: Au-loaded catalyst.

Table 3. Some relevant properties of the samples, as derived by XRD patterns, and Band gap calculation from DR UV-Vis data elaborated according to Tauc plots and N_2 sorption isotherms at -196 ºC

Sample	P25	FSP	0.1 mol% Pd-P25	0.1 mol% Pd-FSP	0.1 mol% Au-P25
Anatase / Rutile (%)	78 / 22	69 / 31	58/42	53/47	78 / 22
Crystallite size (nm) [a]	15	20	17	18	15
Band Gap energy (eV) [b]	3.36	3.36	3.16	3.13	3.12
BET Surface area (m^2/g) [c]	45.3 ± 0.5	67.5 ± 1.2	56.6 ± 0.2	57.0 ± 0.4	47.29 ± 0.17
Total pore volume (cm^3/g) [d]	0.12	0.14	0.25	0.21	0.28
t-Plot micropore volume (cm^3/g) [d]	0.01	0.02	0.004	0.0003	0.003

[a] Crystallite size quantification from XRD data through the Scherrer equation.
[b] as calculated by the Tauc equation for DR-UV-Vis spectra
[c] as calculated from N_2 adsorption/desorption isotherms, collected at -196 °C
[d] as calculated by applying the t-plot.

The FSP procedure led to a similar material than the reference commercial P25 sample, characterized by a mixture of anatase and rutile phases, the latter slightly more abundant in the FSP sample and increasing for the Pd-loaded sample (due to the thermal treatment). The crystal size was also similar, a bit higher for the FSP catalyst according to the Scherrer equation. FE-SEM analysis substantially confirmed the particles size, which was very uniform and centred around 15-30 nm for the P25-based samples, with some poly-dispersity of particles size for the FSP samples, which were mainly constituted by nanospheres (5-20 nm), together with bigger aggregates (*ca.* 100 nm) (Figure 3).

The images of BackScattered electrons are also reported in Figure 4, where brighter dots represent electron denser species (*i.e.* the metals). From these micrographs we can conclude a fine dispersion of the Pd co-catalyst over the whole surface, with very small metal clusters. On the contrary, Au

was characterized by slightly bigger clusters with maximum size 15 nm, *i.e.* covering the whole titania particle.
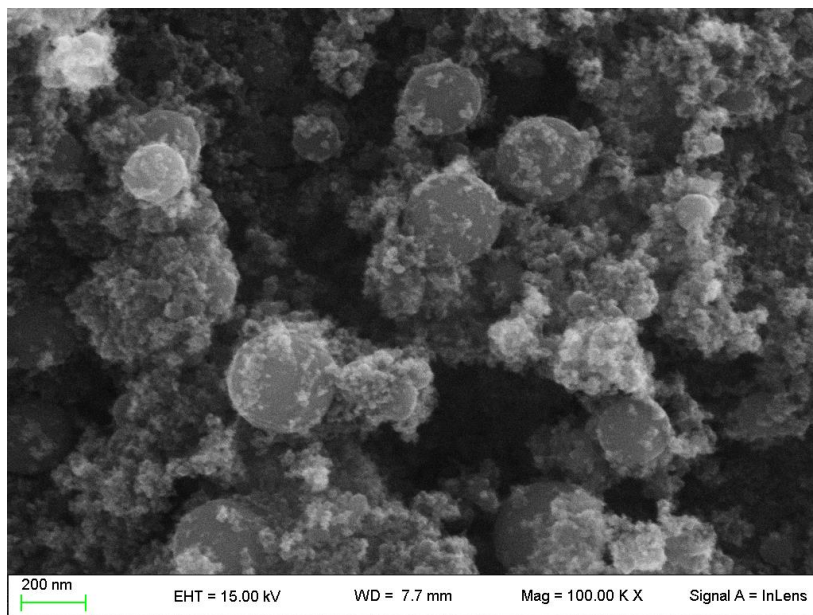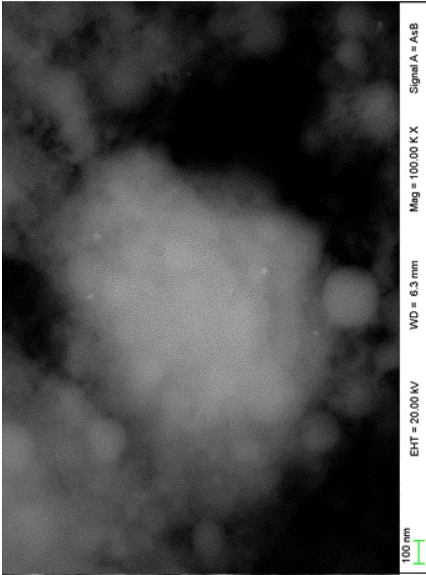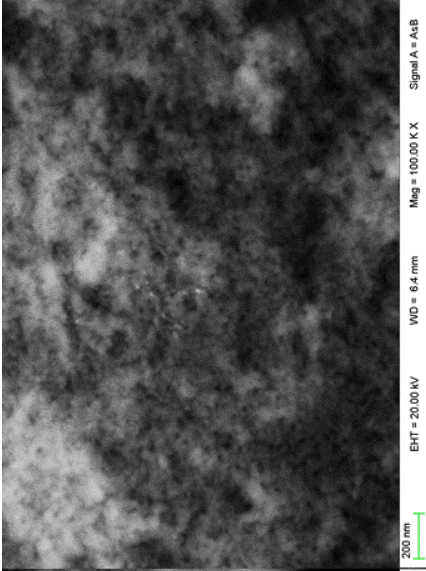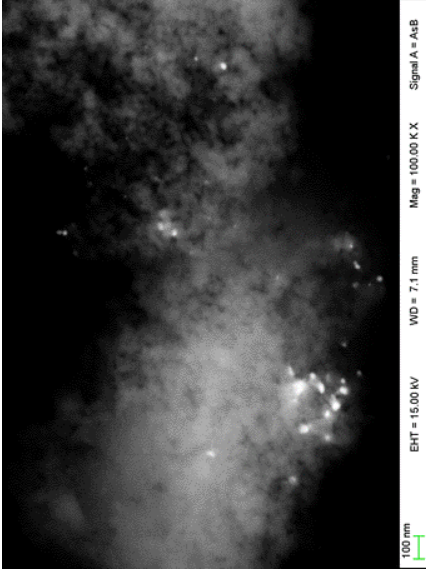
(a)
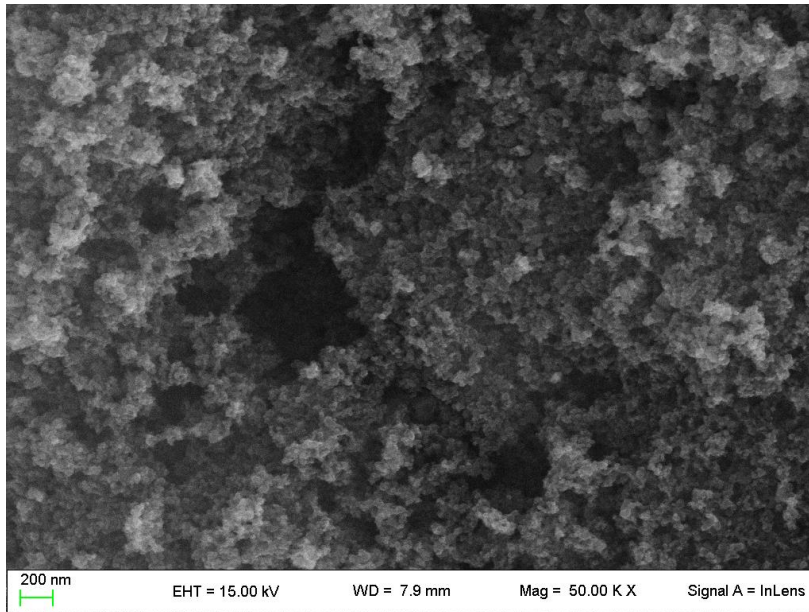
(b)
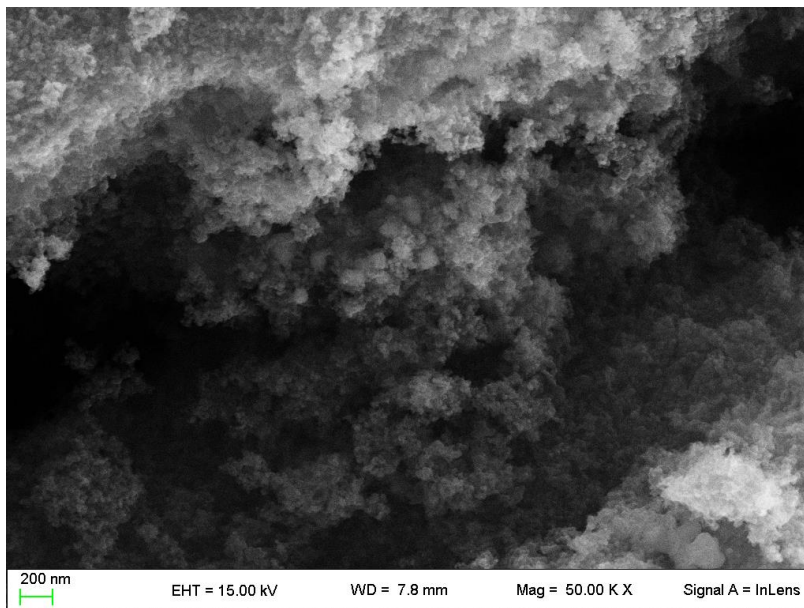
(c)

Figure 3: FE-SEM micrographs of (a) 0.1% Pd-P25, (b) 0.1% Au-P25 and (c) 0.1% Pd-FSP.
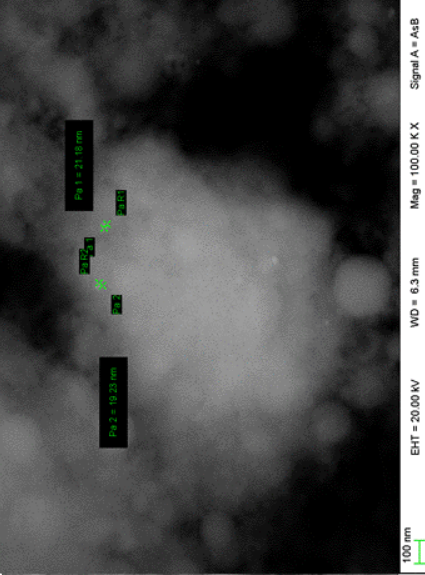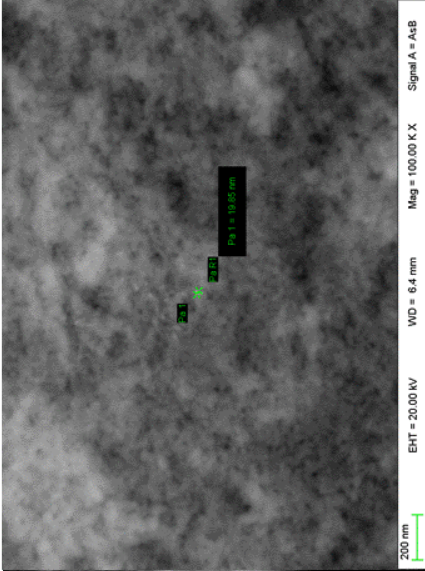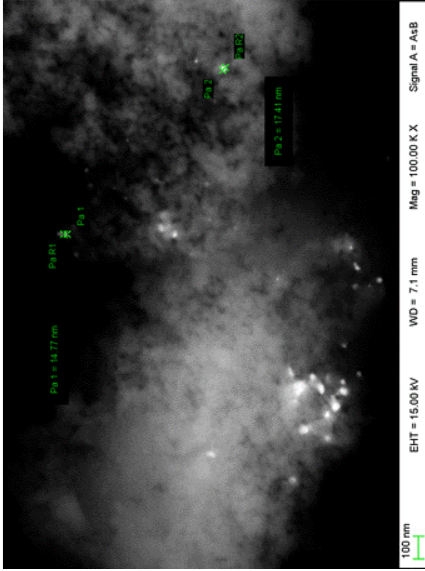
Au- P25

Pd- P25

Pd- FSP

Figure 4: Backscattering images of Pd and Au-loaded samples (brighter dots represent the heavier Pd or Au clusters).

According to UV absorption spectra (Figure 5), all samples show an intense absorption in the spectral range between 240–380 nm, mainly due to electron transfer from the 2p valence band orbital of O to the 3d conduction band orbital of Ti [55,56]. The spectra of un-promoted P25 and FSP samples show lower wavelength cut-off with respect to the metal-loaded samples. The main reason for the observed bathochromic shift in transition and the visible light absorption is due to changing of the energy levels of the semiconductor band gap through a charge transfer between the metal conduction band and the valence band or the d–d transition in the crystal field [52]. Though the band gap quantified through the Tauc elaboration was the same for the bare Titania samples, a higher absorbance was observed for the FSP sample and a slight shift towards higher wavelengths, likely due to a higher rutile content.
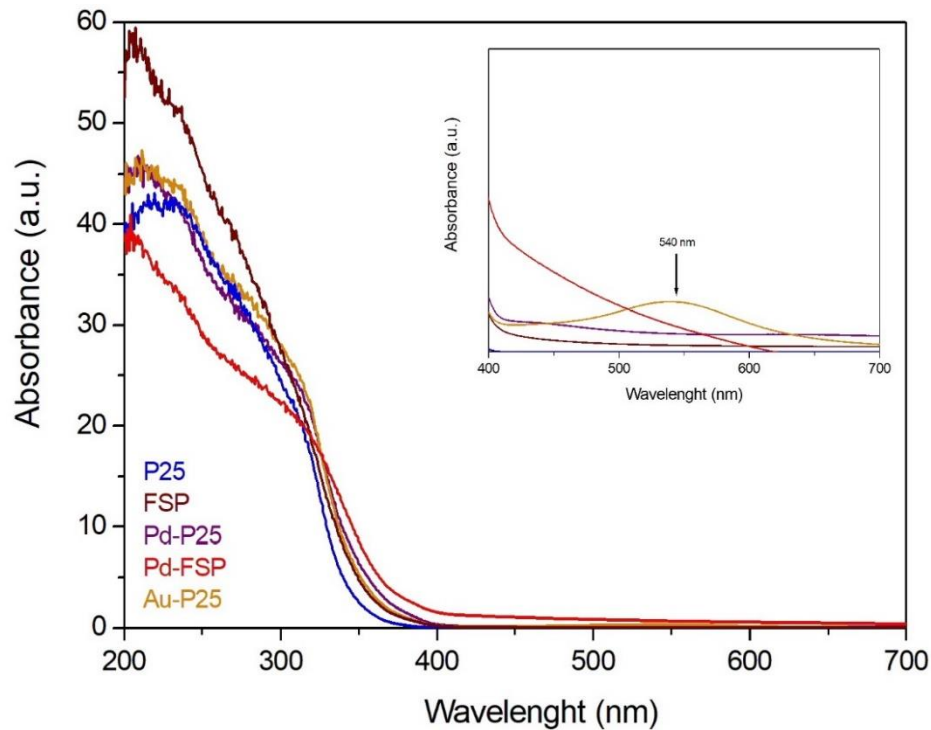
Figure. 5: DR UV-Vis spectra of P25 (blue curve), FSP (dark red curve), Pd-25 (purple curve), Pd-FSP (red curve) and Au-P25 (yellow curve), (all samples were doped with 0.1mol% of Au or Pd).

In addition, Au-TiO$_2$ samples exhibit significantly enhanced light absorption in the visible region showing a broad band located between 450 and 600 nm typical of the Surface Plasmonic Resonance (SPR) of Au nanoparticles (NPs) (*inset* of Figure 5). The broad visible light absorption range is possibly due to wide size distribution of Au-NPs and the maximum of the SPR band (λ_{max}) intensity is mainly related to the size and content of Au particles [57].

The optical band gap energy E$_g$ was determined according to the Tauc equation and reported in Table 3. [58]. According to the E$_g$ calculations, adding Pd or Au to TiO$_2$ results in the extension of absorption edge to longer wavelengths and reduction of the band gap energy [55,59].

The BET SSA (Brunauer-Emmett-Teller Specific Surface Area) and pore volume have been determined based on N$_2$ adsorption/desorption isotherms at -196 °C, on both P25 and FSP samples

previously outgassed at 150 °C for 4h (Figure 6). *t*-plot method has been used for calculation of Micropore volume (Table 3). Both P25 and FSP samples show a type II isotherm, representing the non-porous or macroporous adsorbent (Figure 6) [60]. FSP samples, however, show higher surface area and pore volume with respect to P25 ones. The addition of the metals left almost unaltered the surface area, as for order of magnitude, but decreased by at least one order of magnitude the micropores volume, due to fine pore blocking after addition of the metal nanoparticles.
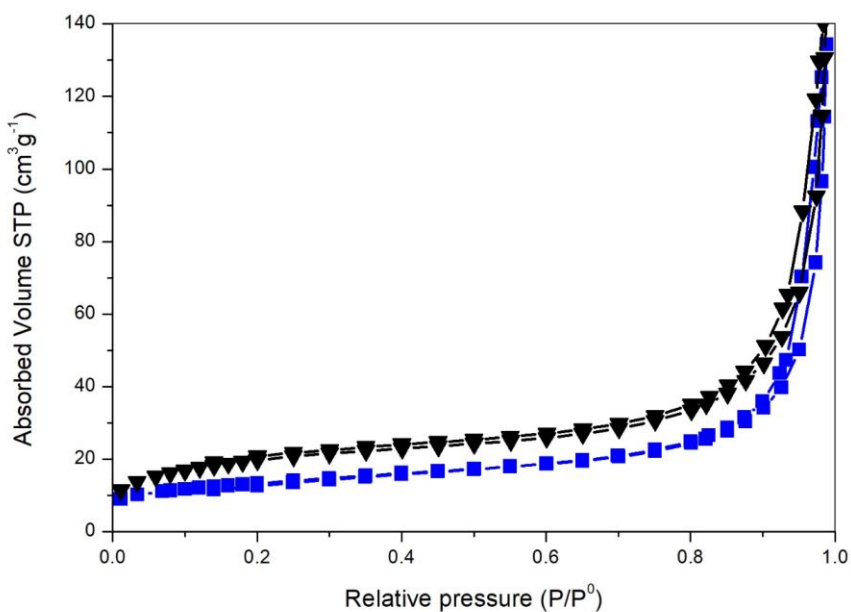
Figure 6: N_2 adsorption/desorption isotherms collected at -196 ºC over samples outgassed at 150°C for 4h, P25 (squares), FSP (triangles)

3.2. Reactivity testing: Effect of dye concentration, H_2O_2 amount and irradiation source type (MP or LP UV lamps)

Figures 7a and 7b, report the discoloration of the model wastewater in the first round of experiments without the presence of heterogeneous catalysts. For all the tests, discoloration nearly follows a first order reaction kinetics and the rate of discoloration can be determined from the

exponent constant factor of the exponential degradation curve, which represents the dye removal rate (Figure 7 and Table 4).

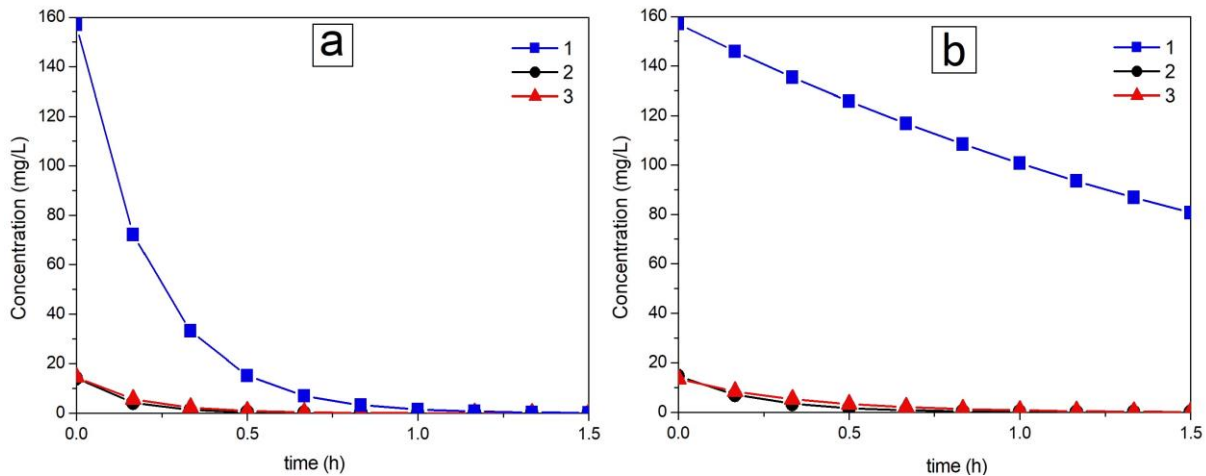Figure 7: Dye concentration evolution with time for a) MP UV-FSR and b) LP UV-FSR. (Curve 1: 150 mg/dm^3 dye and F=5.8 (H_2O_2 addition), curve 2: 10 mg/dm^3 dye and F=5.8 (H_2O_2 addition) and curve 3: 10 mg/dm^3 dye and F=1 (H_2O_2 addition)

The MP-UV FSR system shows always a higher reaction rate constant (RRC) with respect to LP-UV FSR. Especially with high dye concentration the RRC is *ca*. 11 times higher in MP-UV FSR than for the LP case (Figure 8a, and Table 4).

The LP Hg lamp is monochromatic with a fixed wavelength emission at 254 nm, whereas the maximum absorbance of UV radiation by H_2O_2 occurs at about 220 nm and the molar absorption coefficient of H_2O_2 at 254 nm is thus lower than at 220 nm. On the other hand, MP Hg lamp typically produces 200 - 280 nm emission spectra, which is in the proper range for producing higher amount of OH• radicals to react with the substrate dye.

A Reactor Characterization (R_c) number has been introduced as a factor for selecting the best UV source from an economic point of view.

$$8. \quad R_c = \frac{input\ power\ (W)\ \times\ UV-C\ efficiency\ (\%)}{Reactor\ Vol\ (L)}$$

Based on the lamps emission efficiency (Table 1), the R_c number has been calculated for the two different light sources:

$$9. \quad R_{c\ (LP-UV\ FSR)} = \frac{210\ (W) \times 0.35}{10\ (L)} = 7.35\ (W/L)$$

$$10. \quad R_{c\ (MP-UV\ FSR)} = \frac{1700\ (W) \times 0.15}{10\ (L)} = 25.5\ (W/L)$$

The R_C values demonstrate about 3.5 times higher UV-C radiation power per liter of reactor volume for MP UV-FSR with respect to LP one. The calculation of R_C is based on the power input and the efficiency of lamp emission in the desired UVC range. Under equal operating conditions, a higher number of photons with appropriate wavelength increases the concentration of activated hydroxyls.

The RC value can be used to evaluate the R_{WW}, which is equivalent to the power consumption to reach a pre-defined conversion goal, which is assumed as 95% dye decomposition from the model wastewater (Figure 8b). The intended point (95%) has been selected based on previous studies, which have been performed for discoloration of the same dye at the University of Stuttgart.

$$11. \quad R_{WW} = R_c \times t_x\ (KWh/m^3)$$

where t_x is the irradiation time (min) needed for conversion of 95% of the dye (Figure 7, Table 4).
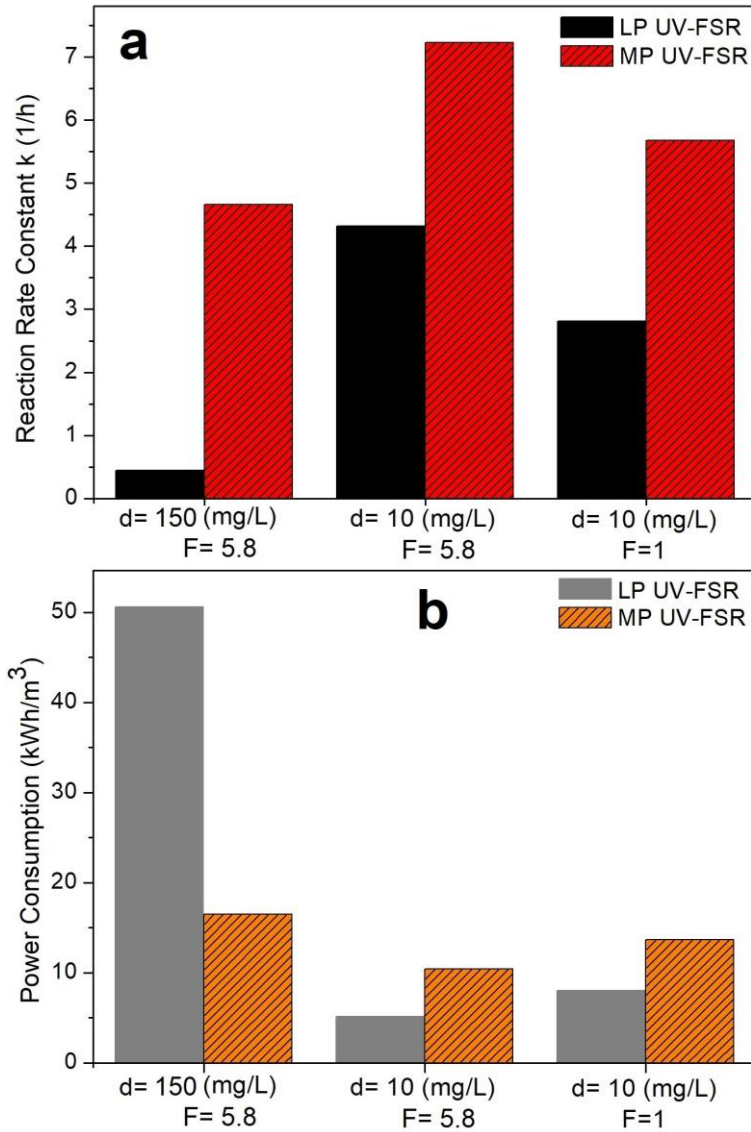
Figure 8: Results of reaction rate constant k (1/h) (a), and Power consumption (kWh/m^3) (b) for different experiments without the presence of an heterogeneous photocatalyst

Table 4: Summary of experiments for tests with and without the presence of an heterogeneous photocatalysts and the results of RRC and R_{ww}

Experiment number	Catalyst	Catalyst Concentration (mg/dm^3)	Dye concentration (mg/dm^3)	UV source	Stoichiometric Factor (F)	H$_2$O$_2$ dosage (cm^3/dm^3)	RRC (1/h)	t$_x$ (min) [*]	R$_{ww}$ (kWh/m^3)
1	No cat	---	10	MP	1	0.017	5.68	31.5	13.40
2	No cat	---	10	MP	5.8	0.1	7.23	24.5	10.41
3	No cat	---	150	MP	5.8	1.5	4.66	38	16.15
4	No cat	---	10	LP	1	0.017	2.81	64	8.00
5	No cat	---	10	LP	5.8	0.1	4.32	41	5.02
6	No cat	---	150	LP	5.8	1.5	0.44	405	50.00
7	No cat	---	100	MP	1.8	0.3	1.13	191	83.0
8	P25	25	100	MP	1.8	0.3	1.74	130	56.4
9	P25	50	100	MP	1.8	0.3	2.25	104	45.2
10	P25	100	100	MP	1.8	0.3	2.33	95	41.4
11	Au-P25	50	100	MP	1.8	0.3	1.91	117	50.5
12	Pd-P25	50	100	MP	1.8	0.3	1.517	142	61.7
13	FSP	50	100	MP	1.8	0.3	1.73	124	53.7
14	Pd-FSP	50	100	MP	1.8	0.3	1.75	123	53.2

[*] irradiation time for 95% of reactive dye removal

According to the values of the R_{ww} (Figure 8b, and Table 4), for removal of the higher concentration (150 mg/dm^3) of Levafix Brilliant Red E-6BA, MP UV-FSR shows a better performance with about 3.5 times less energy consumption with respect to LP UV-FSR.

On the other hand, with a lower dye concentration (10 mg/dm^3) in both over-stoichiometric (F=5.8) and stoichiometric (F=1) conditions, LP UV-FSR requires only half of the energy consumption with respect to the MP UV-FSR, which makes the LP-UV system more economic in such a case. This finding is important for the practical application of the UV/H$_2$O$_2$ process. Several studies have been focused on a degradation of wide range of pollutants, but few studies concern the potential of MP and LP lamps regarding the energy consumption in AOPs systems [61] and therefore their application potential.

Although the absorbance of H$_2$O$_2$ at 254 nm is low, the results of this research show that the yield of hydroxyl radical with LP lamp is almost comparable or even higher at lower dye concentration than the MP lamp.
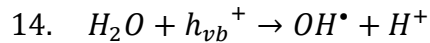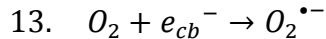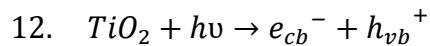
The regulations for the amount of Dissolved Organic Carbon (DOC) and anions (*e.g.* nitrate) for drinking water are specific to each country. However, less than 1-2 mg/dm^3 of DOC is the tolerable range in drinking water. [15]. Although, such low concentrations have no measureable effect on the UV treatment, there is evidence that the presence of nitrate and some parts of the DOC (*e.g.* Natural Organic Matter (NOM)) in the water matrix may act as radical scavengers [49]. It is known that nitrate is able to photolyse when exposed to 254 nm forming radicals (*e.g.* OH• and NO$_2$•). This behavior is mainly due to high molar adsorption coefficient (ε= 3.51 1/M cm) of nitrate at 254 nm that can contribute to high absorption of incident radiation [62]. Furthermore, research studies show the high absorption coefficient of NOM at 254 nm ranging from 116 to 638 1/M cm.

This can be an explanation for our results on the higher efficiency of LP UV-FSR in radical formation, in lower dye concentration [63].

Consequently, with MP-UV/H_2O_2 the influence of direct photolysis assists the degradation of pollutants at the same UV fluence with respect to LP-UV/H_2O_2. Nevertheless, LP-UV/H_2O_2 has higher efficiency in converting the electrical energy to UV-C light, which means the energy required to achieve 95% degradation of reactive dye can be significantly lower with LP-UV/H_2O_2 than with MP-UV/H_2O_2 system, [61,64]. The results of experiments on better performance of LP lamps in a term of power consumption in lower dye concentrations has been clearly illustrated in Figure 8.

3.3.   Effect of heterogeneous photocatalysis on dye removal in MP-UV FSR

The initial step in the semiconductor-mediated photocatalysed degradation is the generation of an electron-hole (e^-/h^+) pair upon light absorption, leading to the formation of a hydroxyl radical (OH•) and superoxide radical ($O_2^{\bullet -}$) anion in solution (equations 12-14). These are the primary oxidizing species in the photocatalytic oxidation processes. For instance, when TiO_2 is used as catalyst:

$$12.\quad TiO_2 + h\upsilon \rightarrow e_{cb}^{\;-} + h_{vb}^{\;+}$$

$$13.\quad O_2 + e_{cb}^{\;-} \rightarrow O_2^{\;\bullet -}$$

$$14.\quad H_2O + h_{vb}^{\;+} \rightarrow OH^{\bullet} + H^+$$

where hυ represents the energy of a radiation higher than the band gap of the semiconductor, e_{cb}^{-} and h_{vb}^{+} represent the electron promoted in the conduction band and the positive hole left in the valence one, respectively. However, the fast electron/hole recombination is also a practical issue with TiO_2 and the main reason of energy-waste, which limits the achievable quantum yield. In

order to inhibit the electron-hole recombination, one strategy is to add electron acceptors, which in turn have several different effects: *i)* to increase the quantity of trapped electrons, therefore, avoid dispersive recombination, *ii)* to generate more radicals and other oxidizing species, *iii)* to increase the oxidation rate of intermediate compounds and *iv)* to compensate problems caused by low oxygen concentration. Furthermore, it may be economically justified the addition of inorganic species to accelerate the degradation rate for highly toxic wastewater. Accordingly, radical chain photo-induced decomposition of hydrogen peroxide as an electron acceptor in pure water produces further OH• and enhances the photodegradation process (equations 1-7).

The effect of catalyst addition on RRC and R_{ww}, has been studied. For all tests, 100 mg/dm^3 and 0.3 cm^3/dm^3 (F=1.8) were selected as dye concentration and H_2O_2 (50 wt%) dosage, respectively. The MP Hg lamp was selected as irradiation source due to better performance for removing the higher concentration of dye. The results of the experiments have been summarized in Table 4.

According to the data, in the presence of heterogeneous photocatalysts the RRC values increased, with a corresponding decrease of power consumption. The best performance for the same amount of catalyst (50 mg/dm^3) has been obtained with P25, leading to almost half power consumption with respect to the test in the same conditions but without catalyst. As expected, the dye discoloration rate has been found to increase with the increase in catalyst concentration from 25 mg/dm^3 to 50 mg/dm^3. The reason is due to increasing active surface sites in the reactor, whereas a further increase of catalyst concentration was not so effective.

The higher photocatalytic activity of Evonik P25 with respect to FSP at the same amount of catalyst can be attributed to the surface charge properties of these photocatalysts. For P25 and FSP, the ζ-potential curves at variable pH allowed to calculate the point of zero charge (PZC). It was calculated as pH 6.25 and 4.5 for P25 and FSP, respectively [54]. Due to the low pK$_a$ value of the

sulfonic group in Levafix Brilliant E-6BA, it is found in its anionic form within the pH range of our experiments (pH 7). Therefore, at pH 7, the surface of FSP catalyst is charged negatively, hampering the adsorption of Levafix Brilliant E-6BA ions and ultimately leading to electrostatic repulsion, which indeed results in lower photodegradation efficiency with respect to P25, which is only slightly negatively charged at pH 7, a pH very near to the isoelectric point of this material [22,65].

Operation with an almost neutrally charged surface may however induce agglomeration and unstable suspension. This could be a problem for sample P25 tested at pH = 7, *i.e.* near to the isoelectric point. To exclude this issue, we have measured the size of the particles in suspension through DLS. The experimental evidence does not report any significant agglomeration of the suspension as a function of pH in the adopted conditions (also thanks to the very low catalyst concentration employed) (Figure 9). The choice to keep unmodified the native pH is favourable from the applicative point of view to avoid the addition of acids and bases to waste water, which would imply and additional post treatment to remove them.
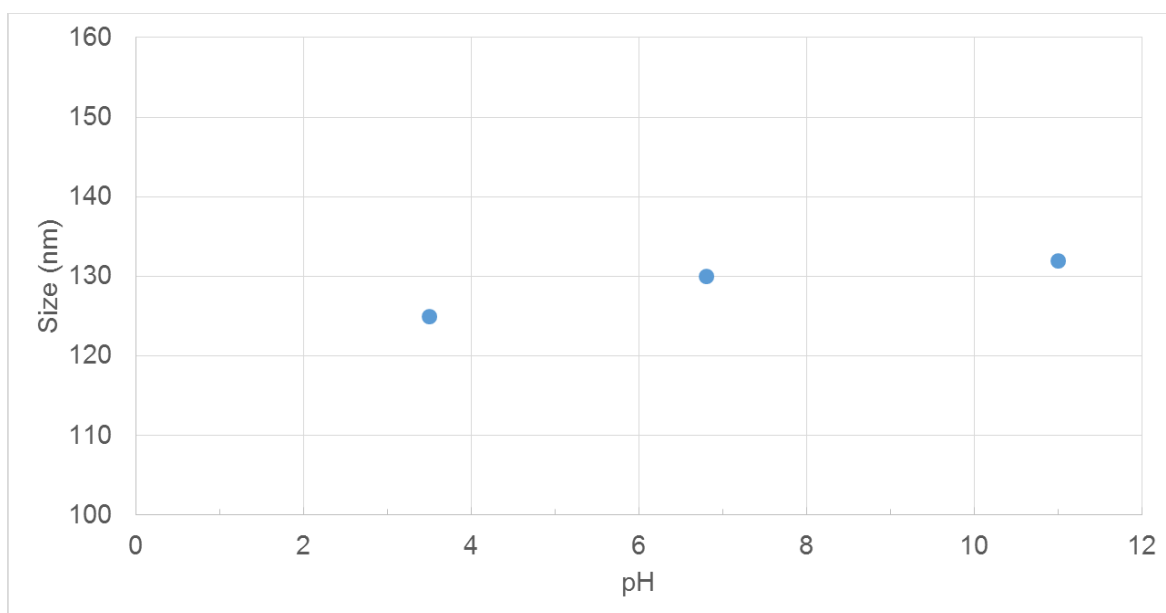
Figure 9: Size of the particles in suspension as measured by DLS as a function of pH.

On the other hand, gold and palladium doping (Pd-P25, Au-P25 and Pd-FSP), seems not to affect the performance significantly. Indeed, in this type of reaction, the effect of metal entrapment for the electrons photogenerated is by far less efficient than usual, given the presence of a very efficient electron scavenger such as H_2O_2 (Table 4). Thus, the net effect of the metal is a reduction of the active TiO_2 surface without any specific advantage.

The UV spectrum of Levafix Brilliant E-6BA is presented in Figure 10. In water, the hydrazone form of Levafix Brilliant E-6BA, stable in the solid phase, undergoes an azo-hydrazone tautomerism, via an intra-molecular proton transfer, so that both hydrazone and azo-form are simultaneously present. Levafix Brilliant E-6BA exhibits peaks at 543, 519, 370, 328 nm and a small shoulder at 288 nm (Figure 10). The visible spectrum peaks are due to chromophoric group absorptions, whereas the bands observed in the UV region can be assigned to the aromatic rings present in dye structures [66,67].
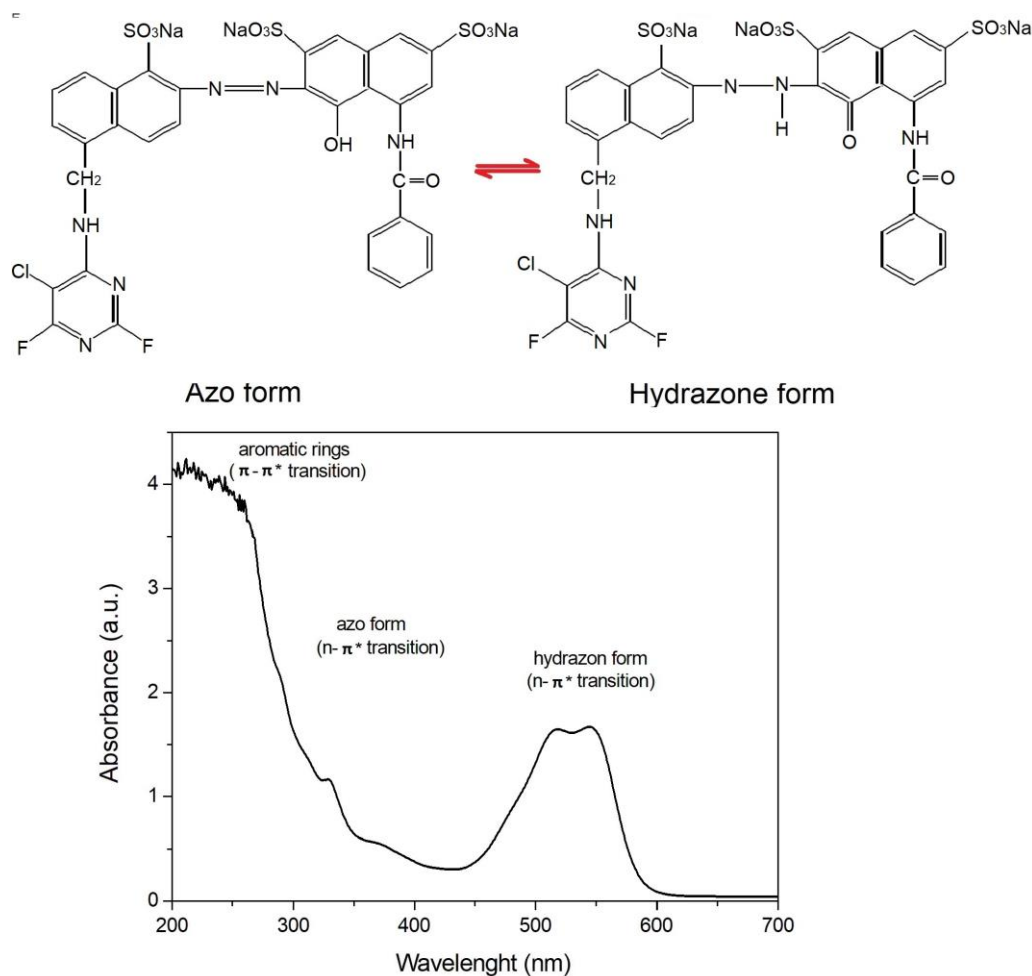
Figure 10: (up) Structure formula of Levafix Brilliant E-6BA. (down) UV–vis spectrum of 0.48 mM Levafix Brilliant E-6BA aqueous solution: absorption bands due to both the azo- and hydrazone forms- of the dye are observed (the dye structure has been adapted from *Muthuraman et al.,* [68]).

Figure 11 describes the adsorption experiments of Levafix Brilliant E-6BA without P25 and with the best amount of P25 (100 mg/dm^3). After 90 min of irradiation, 51% and 21% of dye were converted with 100 mg L^{-1} of P25 and without P25, respectively. The same Figure 11 also demonstrates the effect of dye adsorption in the surface of the catalyst, which is negligible, *i.e.* < 5% when comparing curves 1 and 2.
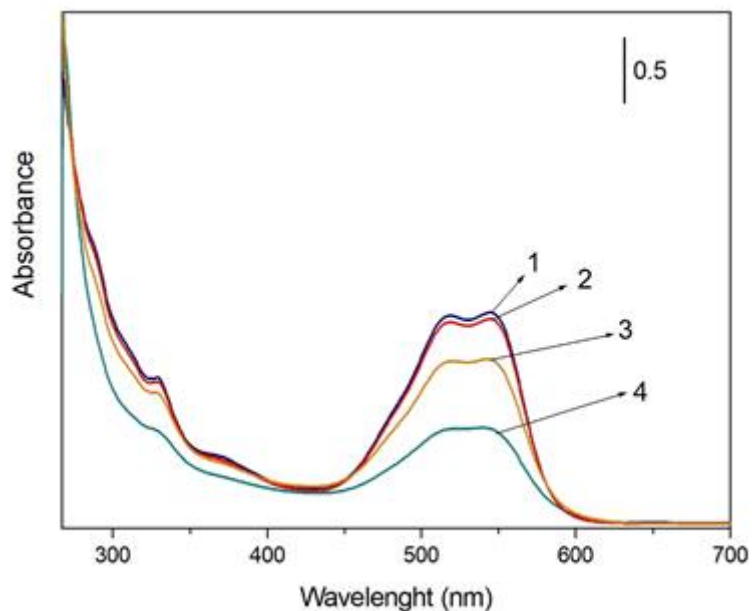
Figure 11: a) UV–vis spectra of the starting 0.48 mM Levafix Brilliant E-6BA solution with 0.3 cm^3/dm^3 H_2O_2 (1) and with 100 mg/dm^3 P25 (2), and of the supernatant solutions after 90 min without the presence of P25 (3) and with 100 mg/dm^3 P25 (4).

The color loss of the dye solution was interpreted with the cleavage of the azo linkage (nitrogen double bonds -N=N-) in the molecule (Figure 10). Azo bonds are the most active bonds in azo dye molecules and can be easily oxidized either by positive holes in the valence band of the semiconductor catalyst or by action of the hydroxyl radicals [69,70].

After 90 min of irradiation time no new bands form with respect to the starting solution. Higher decoloration and degradation of the aromatic structures have been observed in the presence of catalyst P25 (Figure 11). This is visible by looking at the decrease of the typical absorption bands at 288 and 328 nm.

4. Conclusions

A UV Free-Surface reactor (UV-FSR) has been used for studying the photodegradation of Levafix Brilliant E-6BA, a hardly biodegradable anionic reactive azo-dye. Experiments with model wastewater including different concentrations of dye and H_2O_2 as oxidative agent were performed with both medium pressure (MP) UV radiator (1700 W) and low pressure (LP) UV radiator (210 W). Comparing the Reactor characterization number (R_c) values for both sources of UV light, UV-C radiation power per liter was 3 times higher with MP UV-FSR than with LP UV-FSR. The R_{ww} factor, calculated as energy consumption for dye degradation, has been obtained 3 times less for treatment of high amount of dye concentrations in with MP UV-FSR than LP UV-FSR. The MP Hg lamp produced a higher quantity of radicals than LP Hg one, however, with lower concentrations of dye, the radicals termination with recombination or quench process is dominating with respect to dye degradation. Therefore, at lower concentration of dye (10 mg/dm^3), LP UV-FSR shows better performance for energy consumption with different amounts of H_2O_2 dosage (H_2O_2 dosage with two stoichiometry factors of 1 and 5.8), which may have an influence on the results.

Catalyst effect on dye photodegradation has been also studied with 100 mg/dm^3 of dye concentration and H_2O_2 stoichiometry factor of 1.8. Interestingly, bare TiO_2 (P25) even in relatively low quantity (100 mg/dm^3, while literature often reports concentrations of *ca.* 1 g/dm^3 for photocatalytic applications) showed to be an active co-adjuvant for decoloration and aromatic structures degradation of the dye with half the energy consumption with respect to a solution without heterogeneous catalyst. The FSP catalyst, instead, showed lower performance, leading to higher energy consumption than P25. This result may be attributed to the surface charge conditions and the isoelectric point of the two catalysts, as determined by ζ-potential curves. The selected pH

for this study has been set as neutral (pH = 7), in which P25 has less negative surface charge with respect to FSP. Therefore, repulsive electrostatic interaction is established between the anionic form of the dye at that pH and the negative catalyst surface of FSP TiO_2, which explains the lower photocatalytic activity for this latter catalyst.

Adding noble metals as co-catalysts (*ca.* 0.1 mol% Pd or Au) has no significant effect on the catalysts efficiency. Metals are indeed effective to entrap electrons preventing their recombination with holes. In this case, H_2O_2 was much more efficient as electron scavenger leading to a negligible or even negative effect of the metal.

ACKNOWLEDGEMENTS

References

[1]   G. Mishra, M. Tripathy, A Critical Review of the Treatments for Decolourization of Textile Effluent, Colorage. (1993) 35–38.

[2]   B.H.A.I. Tan, T.T.O.W. Teng, A.K.M.O. M, REMOVAL OF DYES AND INDUSTRIAL DYE WASTES BY MAGNESIUM CHLORIDE, Water Res. 34 (2000) 597–601.

[3]   A.Z. Bouyakoub, B.S. Lartiges, R. Ouhib, S. Kacha, A.G. El Samrani, J. Ghanbaja, et al., MnCl 2 and MgCl 2 for the removal of reactive dye Levafix Brilliant Blue EBRA from synthetic textile wastewaters : An adsorption / aggregation mechanism, J. Hazard. Mater. 187 (2011) 264–273. doi:10.1016/j.jhazmat.2011.01.008.

[4]   S.M. Palácio, F.R. Espinoza-qui, A.N. Módenes, C.C. Oliveira, F.H. Borba, F.G.S. Jr, Toxicity assessment from electro-coagulation treated-textile dye wastewaters by bioassays, J. Hazard. Mater. J. 172 (2009) 330–337. doi:10.1016/j.jhazmat.2009.07.015.

[5]   T. Kurbus, Y. March, A. Majcen, L. Marechal, The use of experimental design for the evaluation of the influence of variables on the H2O2/UV treatment of model textile waste water, Dye. Pigment. 58 (2003) 171–178. doi:10.1016/S0143-7208(03)00054-8.

[6]   S. Kang, C.-H. Liao, H.-P. Hung, Peroxidation treatment of dye manufacturing wastewater in the presence of ultraviolet light and ferrous ions, J. Hazard. Mater. B65 (1999) 317–333.

[7]   P.K. Malik, S.K. Saha, Oxidation of direct dyes with hydrogen peroxide using ferrous ion as catalyst, Sep. Purif. Technol. 31 (2003) 241–250.

[8]   E. Bahadori, V. Vaiano, S. Esposito, M. Armandi, D. Sannino, Photo-activated degradation of tartrazine by H 2 O 2 as catalyzed by both bare and Fe-doped methyl-imogolite nanotubes, Catal. Today. 304 (2018) 199–207. doi:10.1016/j.cattod.2017.08.003.

[9]   E. Shafia, S. Esposito, M. Armandi, E. Bahadori, E. Garrone, B. Bonelli, Reactivity of bare and Fe-doped alumino-silicate nanotubes (imogolite) with H 2 O 2 and the azo-dye Acid Orange 7,

Catal. Today. 277 (2016) 89–96. doi:10.1016/j.cattod.2015.10.011.

[10]   G. Ciardelli, G. Brighetti, N. Ranieri, Oxidation and separation treatment for textile wastewaters recycling, Proc. TMS Fall Extr. Process Conf. 3 (1999) 2357–2366.

[11]   H. Mirbolooki, R. Amirnezhad, A. Reza, Treatment of high saline textile wastewater by activated sludge microorganisms, Rev. Mex. Trastor. Aliment. 15 (2017) 167–172. doi:10.1016/j.jart.2017.01.012.

[12]   M. Sala, M.C. Gutiérrez-Bouzàn, Electrochemical Techniques in Textile Processes and Wastewater Treatment, Int. J. Photoenergy. (2012). doi:10.1155/2012/629103.

[13]   X. Zhu, J. Ni, J. Wei, X. Xing, H. Li, Destination of organic pollutants during electrochemical oxidation of biologically-pretreated dye wastewater using boron-doped diamond anode, J. Hazard. Mater. 189 (2011) 127–133. doi:10.1016/j.jhazmat.2011.02.008.

[14]   I. Oller, S. Malato, J.A. Sánchez-pérez, Science of the Total Environment Combination of Advanced Oxidation Processes and biological treatments for wastewater decontamination — A review, Sci. Total Environ. 409 (2011) 4141–4166. doi:10.1016/j.scitotenv.2010.08.061.

[15]   T. Oppenländer, Photochemical purification of water and air, 2003 WILEY-VCH Verlag GmbH & Co., 2007. doi:https://doi.org/10.1002/9783527610884.ch.

[16]   I.K. Konstantinou, T.A. Albanis, TiO2 -assisted photocatalytic degradation of azo dyes in aqueous solution : kinetic and mechanistic investigations A review, Appl. Catal. B Environ. 49 (2004) 1–14. doi:10.1016/j.apcatb.2003.11.010.

[17]   M.R. Hoffmann, S.T. Martin, W. Choi, D.W. Bahnemannt, Environmental Applications of Semiconductor Photocatalysis, Chem.Rev. 95 (1995) 69–96. doi:10.1021/cr00033a004.

[18]   J. Beltran, D. Heredia, J. Torregrosa, J.R. Dominguez, J.A. Peres, Oxidation of p -hydroxybenzoic acid by UV radiation and by TiO2/UV radiation : comparison and modelling of reaction kinetic, J. Hazard. Mater. B83 (2001) 255–264.

[19]   A. V Vorontsov, V.P. Dubovitskaya, Selectivity of photocatalytic oxidation of gaseous ethanol over pure and modified TiO2, J. Catal. 221 (2004) 102–109. doi:10.1016/j.jcat.2003.09.011.

[20]   F.S. Freyria, M. Armandi, M. Compagnoni, G. Ramis, I. Rossetti, B. Bonelli, Catalytic and photocatalytic processes for the abatement of N-containing pollutants from wastewater. Part 2: Organic pollutants, J. Nanosci. Nanotechnol. 17 (2017) 3654–3672. doi:10.1166/jnn.2017.14014.

[21]   D. Chen, A.K. Ray, D. Chen, A.K. Ray, PHOTODEGRADATION KINETICS OF 4-NITROPHENOL IN TiO2 SUSPENSION, Wat. Res. 32 (1998) 3223–3234.

[22]   M. Saquib, M. Muneer, Titanium dioxide mediated photocatalyzed degradation of a textile dye derivative , acid orange 8 , in aqueous suspensions, Desalination. 155 (2003) 255–263.

[23]   C. Bauer, P. Jacques, A. Kalt, Photooxidation of an azo dye induced by visible light incident on the surface of TiO2, J. Photochem. Photobiol. A Chem. 140 (2001) 87–92.

[24]   F.S. Freyria, M. Compagnoni, N. Ditaranto, I. Rossetti, M. Piumetti, G. Ramis, et al., Both pure and Fe doped mesoporous titania catalyse the oxidation of Acid Orange 7 by H_2O_2 in different experimental conditions, Catalysts. 7 (2017) 213.

[25]   E. Bahadori, V. Vaiano, S. Esposito, M. Armandi, D. Sannino, Photo-activated degradation of tartrazine by H_2O_2 as catalyzed by both bare and Fe-doped methyl-imogolite nanotubes, Catal. Today. 304 (2018) 199–207. doi:10.1016/j.cattod.2017.08.003.

[26]   S.. Penner, Steps toward the hydrogen economy, Energy. 31 (2006) 33–43.

[27]   H.-J. Choi, M. Kang, Hydrogen production from methanol/water decomposition in a liquid photosystem using the anatase structure of Cu loaded TiO2, Int. J. Hydrogen Energy. 32 (2007) 3841–3848.

[28]   L.S. Yoong, F.. Chong, B.. Dutta, Development of copper-doped TiO2 photocatalyst for hydrogen production under visible light, Energy. 34 (2009) 1652–1661.

[29]   B.-R. Chen, V.-H. Nguyen, J.C.S. Wu, R. Martin, K. Kočí, Production of renewable fuels by the photohydrogenation of CO2: effect of the Cu species loaded onto TiO2 photocatalysts., Phys. Chem. Chem. Phys. 18 (2016) 4942–51. doi:10.1039/c5cp06999h.

[30]   K. Koci, K. Matteju, L. Obalovà, S. Krejcikovà, Z. Lacny, D. Plachà, et al., Effect of silver doping on the TiO2 for photocatalytic reduction of CO2, Appl. Catal. B Environ. 96 (2010) 239–244.

doi:10.1016/j.apcatb.2010.02.030.

[31]   M. Compagnoni, G. Ramis, F.S. Freyria, M. Armandi, B. Bonelli, I. Rossetti, Photocatalytic

        processes for the abatement of N-containing pollutants from waste water. Part 1: Inorganic

        pollutants, J. Nanosci. Nanotechnol. 17 (2017) 3632–3653.

[32]   E. Bahadori, M. Compagnoni, A. Tripodi, F. Freyri, M. Armandi, B. Bonelli, et al.,

        Photoreduction of nitrates from waste and drinking water, Mater. Today Proc. 5 (2018) 17404–

        17413.

[33]   R. Salazar, J. Gallardo-Arriaza, J. Vidal, C. Rivera-Vera, C. Toledo-Neira, M.A. Sandoval, et al.,

        Treatment of industrial textile wastewater by the solar photoelectro-Fenton process: Influence of

        solar radiation and applied current, Sol. Energy. 190 (2019) 82–91.

        doi:10.1016/j.solener.2019.07.072.

[34]   S.K. Sen, P. Patra, C.R. Das, S. Raut, S. Raut, Pilot-scale evaluation of bio-decolorization and

        biodegradation of reactive textile wastewater: An impact on its use in irrigation of wheat crop,

        Water Resour. Ind. 21 (2019) 100106. doi:10.1016/j.wri.2019.100106.

[35]   F. Masi, A. Rizzo, R. Bresciani, N. Martinuzzi, S.D. Wallace, D. Van Oirschot, et al., Lessons

        learnt from a pilot study on residual dye removal by an aerated treatment wetland, Sci. Total

        Environ. 648 (2019) 144–152. doi:10.1016/j.scitotenv.2018.08.113.

[36]   M. Compagnoni, J. Lasso, A.I. Di Michele, I. Rossetti, Catalysis Science & Technology Flame-

        pyrolysis-prepared catalysts for the steam reforming of ethanol, Catal. Sci. Technol. 6 (2016)

        6247–6256. doi:10.1039/C5CY01958C.

[37]   G.L. Chiarello, I. Rossetti, L. Forni, Flame-spray pyrolysis preparation of perovskites for methane

        catalytic combustion, J. Catal. 236 (2005) 251–261.

[38]   I. Rossetti, L. Fabbrini, N. Ballarini, C. Oliva, F. Cavani, A. Cericola, et al., V-Al-O catalysts

        prepared by flame pyrolysis for the oxidative dehydrogenation of propane to propylene, Catal.

        Today. 141 (2009) 271–281. doi:10.1016/j.cattod.2008.05.020.

[39]   G.L. Chiarello, I. Rossetti, L. Forni, P. Lopinto, G. Migliavacca, Solvent nature effect in

preparation of perovskites by flame-pyrolysis. 1. Carboxylic acids, Appl. Catal. B Environ. 72 (2007) 218–226. doi:10.1016/j.apcatb.2006.11.001.

[40] G.L. Chiarello, I. Rossetti, L. Forni, P. Lopinto, G. Migliavacca, Solvent nature effect in preparation of perovskites by flame pyrolysis. 2. Alcohols and alcohols + propionic acid mixtures, Appl. Catal. B Environ. 72 (2007) 227–232. doi:10.1016/j.apcatb.2006.10.026.

[41] G.L. Chiarello, I. Rossetti, L. Forni, Flame-spray pyrolysis preparation of perovskites for methane catalytic combustion, J. Catal. 236 (2005) 251–261. doi:10.1016/j.jcat.2005.10.003.

[42] G.L. Chiarello, I. Rossetti, P. Lopinto, G. Migliavacca, L. Forni, Preparation by flame spray pyrolysis of ABO3±δ catalysts for the flameless combustion of methane, Catal. Today. 117 (2006) 549–553. doi:10.1016/j.cattod.2006.06.018.

[43] I. Rossetti, A. Villa, M. Compagnoni, L. Prati, G. Ramis, C. Pirola, et al., CO2 photoconversion to fuels under high pressure: effect of TiO2 phase and of unconventional reaction conditions, Catal. Sci. Technol. 5 (2015) 4481–4487. doi:10.1039/C5CY00756A.

[44] E. Bahadori, A. Tripodi, A. Villa, C. Pirola, L. Prati, G. Ramis, et al., High Pressure Photoreduction of CO2: Effect of Catalyst Formulation, Hole Scavenger Addition and Operating Conditions, Catalysts. 8 (2018) 430. doi:10.3390/catal8100430.

[45] E. Bahdori, A. Tripodi, A. Villa, C. Pirola, L. Prati, G. Ramis, et al., High pressure CO2 photoreduction using Au/TiO2: unravelling the effect of the co-catalyst and of the titania polymorph, Catal. Sci. Technol. 9 (2019) 2253–2265.

[46] M. Compagnoni, S.A. Kondrat, C.E. Chan-Thaw, D.J. Morgan, D. Wang, L. Prati, et al., Spectroscopic Investigation of Titania-Supported Gold Nanoparticles Prepared by a Modified Deposition/Precipitation Method for the Oxidation of CO, ChemCatChem. 8 (2016). doi:10.1002/cctc.201600072.

[47] N. Baycan, E. Thomanetz, F. Sengül, Influence of chloride concentration on the formation of AOX in UV oxidative system, J. Hazard. Mater. 143 (2007) 171–176.

[48] G.W. Vanloon, S.J. Duffy, Environmental Chemistry: A global perspective, Oxford University,

Oxford, 2000.

[49]   E. Lipczynska-kochany, G. Sprah, S. Harms, INFLUENCE OF SOME GROUNDWATER AND
        SURFACE WATERS CONSTITUENTS ON THE DEGRADATION OF 4-CHLOROPHENOL
        BY THE FENTON REACTION, Chemosphere. 30 (1995) 9–20.

[50]   K. Thamaphat, P. Limsuwan, B. Ngotaworncai, Phase Characterization of TiO 2 Powder by XRD
        and TEM, 361 (2008) 357–361.

[51]   R.A. Spurr, H. Myers, Quantitative Analysis of Anatase-Rutile Mixtures with an X-Ray
        Diffractometer, (n.d.) 760–762. doi:10.1021/ac60125a006.

[52]   R. Chauhan, A. Kumar, R.P. Chaudhary, Structural and optical characterization of Ag-doped TiO
        2 nanoparticles prepared by a sol – gel method, (2012) 1443–1453. doi:10.1007/s11164-011-0475-
        8.

[53]   E. Bahadori, M. Compagnoni, A. Tripodi, F. Freyria, M. Armandi, B. Bonelli, et al.,
        Photoreduction of nitrates from waste and drinking water, Mater. Today Proc. 5 (2018) 17404–
        17413. doi:10.1016/j.matpr.2018.06.042.

[54]   E. Bahadori, A. Tripodi, G. Ramis, I. Rossetti, Semibatch photocatalytic reduction of nitrates: role
        of process conditions and co-catalysts, ChemCatChem. in press (2019).
        doi:10.1002/cctc.201900890.

[55]   S. N, K. E, Synthesis of Mesoporous Pd-Doped TiO2 Templated by a Magnetic Recyclable Ionic
        Liquid for Efficient Photocatalytic Air Treatment, Ind. Eng. Chem. Res. 55 (2016) 10533–10543.

[56]   S. Tan, B.. Chen, W. Sun, X, W.J. Fan, H.S. Kwok, X.H. Zhang, Blueshift of optical band gap in
        ZnO thin films grown by metal-organic chemical-vapor deposition, J. Appl. Phys. 98 (2005)
        013505.

[57]   M. Compagnoni, A. Villa, E. Bahdori, D.J. Morgan, L. Prati, N. Dimitratos, et al., Surface probing
        by spectroscopy on titania-supported gold nanoparticles for a photo-reductive application, Appl.
        Catal. A Gen. (2018).

[58]   P. Li, H. Hu, J. Xu, H. Jing, H. Peng, J. Lu, New insights into the photo-enhanced electrocatalytic

reduction of carbon dioxide on MoS2-rods/TiO2 NTs with unmatched energy band, Appl. Catal., B Env. 147 (2014) 912–919.

[59] S.I. Mogal, V.G. Gandhi, M. Mishra, S. Tripathi, T. Shripathi, P.. Joshi, et al., Single-Step Synthesis of Silver-Doped Titanium Dioxide: Influence of Silver on Structural, Textural, and Photocatalytic Properties, Ind. Eng. Chem. Res. 53 (2014) 5749–5758.

[60] M. Thommes, K. Kaneko, A. V Neimark, J.P. Olivier, F. Rodriguez-reinoso, J. Rouquerol, et al., Physisorption of gases , with special reference to the evaluation of surface area and pore size distribution (IUPAC Technical Report), 87 (2015) 1051–1069. doi:10.1515/pac-2014-1117.

[61] G.F. IJpelaar, D.J.H. Harmsen, E.F. Beerendonk, R.C. Van Leerdam, D.H. Metz, A.H. Knol, Comparison of Low Pressure and Medium Pressure UV Lamps for UV/H2O2 Treatment of Natural Waters Containing Micro Pollutants, J. Int. Ozone Assoc. 32 (2010) 329–337.

[62] Oliver C Zafiriou, M.B. True, Nitrate photolysis in seawater by sunlight, Mar. Chem. 8 (1979) 33–42.

[63] C. Duca, Effect of water matrix on Vacuum UV process for the removal of organic micropollutants in surface water (T)., Univ. Br. Columbia. Retrieved from Https//Open.Library.Ubc.ca/Collections/Ubctheses/24/Items/1.0167680. (2015).

[64] K.M.S. Hansen, R. Zortea, A. Piketty, S. Rodriguez, H. Rasmus, Science of the Total Environment Photolytic removal of DBPs by medium pressure UV in swimming pool water, Sci. Total Environ. 443 (2013) 850–856. doi:10.1016/j.scitotenv.2012.11.064.

[65] S. Banerjee, M.C. Chattopadhyaya, Adsorption characteristics for the removal of a toxic dye, tartrazine from aqueous solutions by a low cost agricultural by-product, Arab. J. Chem. 10 (2017) S1629–S1638.

[66] S. Mozia, M. Tomaszewska, A.W. Morawski, Photodegradation of azo dye Acid Red 18 in a quartz labyrinth flow reactor with immobilized TiO2 bed, Dye. Pigment. 75 (2007) 60–66. doi:10.1016/j.dyepig.2006.05.012.

[67] H. Al-ekabi, N. Serpone, Kinetic Studies in Heterogeneous Photocatalysis . 1 . Photocatalytic

Degradation of Chlorinated Phenols in Aerated Aqueous Solutions over Ti02 Supported on a Glass Matrix, J. Mater. Chem. 92 (1988) 5726–5731. doi:10.1021/j100331a036.

[68]   G. Muthuraman, M. Sathya, M. Soniya, S. Elumalai, Recovery of Levafix brilliant red E-4BA and Levafix brilliant red E-6BA from aqueous solution by supported liquid membrane, Membr. Water Treat. 4 (2013) 227.

[69]   W. Feng, D. Nansheng, H. Helin, Degradation mechanism of azo dye C . I . reactive red 2 by iron powder reduction and photooxidation in aqueous solutions, Chemosphere. 41 (2000) 0–5.

[70]   M. Karkmaz, E. Puzenat, C. Guillard, J.M. Herrmann, Photocatalytic degradation of the alimentary azo dye amaranth Mineralization of the azo group to nitrogen, Appl. Catal., B Env. 51 (2004) 183–194. doi:10.1016/j.apcatb.2004.02.009.